Materials Science and Engineering C 29 (2009) 2085–2091

Contents lists available at ScienceDirect

Materials Science and Engineering C

journal homepage: www.elsevier.com/locate/msec

Physico/chemical characterization and preliminary human histology assessment of a β-TCP particulate material for bone augmentation

Paulo G. Coelho [a,*], Maria E. Coimbra [a,b], Cristiane Ribeiro [c], Elizabeth Fancio [c], Olga Higa [c], Marcelo Suzuki [d], Mauro Marincola [e,f]

[a] Department of Biomaterial and Biomimetics, New York University, College of Dentistry, New York, NY, 10100, USA
[b] Department of Materials Science, Instituto Militar de Engenharia (IME), Rio de Janeiro, RJ, Brazil
[c] IPEN — Instituto de Pesquisa Energéticas e Nucleares, University of São Paulo, São Paulo, Brazil
[d] Dept. of Prosthodontics, Tufts University School of Dental Medicine, Boston, USA
[e] Private Practice, Rome, Italy
[f] University of Cartagena, Cartagena, Colombia

ARTICLE INFO

Article history:
Received 4 September 2008
Received in revised form 17 December 2008
Accepted 9 April 2009
Available online 23 April 2009

Keywords:
β-TCP
Physicho/chemical characterization
Biocompatibility
In vitro test
Human histology

ABSTRACT

This study aimed to physico/chemically characterize and evaluate the in vivo performance of a β-TCP particulate grafting material. SEM/TEM, and EDS and XPS were used for morphology and chemistry assessment, respectively. FTIR was used to determine Ca–P phases characteristic bands. Rietveld refinement/XRD spectra was performed for secondary phase detection. Particle size distribution and specific surface were assessed by a scattering-laser based technique and BET, respectively. Mercury porosimetry was employed to determine pore-size distribution. For in vivo evaluation, the grafting material was used in 12 patients' sinus lifts, and biopsies were obtained at post-operative times of 3, 6, and 9 months. SEM/TEM revealed multigrained particles with interconnected pores. EDS showed Ca, P, and O, with stoichiometry close to theoretical values. XRD/Rietveld showed that the material presented crystalline β-TCP with ~9% β-$Ca_2P_2O_7$ secondary phase. FTIR did not detect the presence of bands related to α-TCP. Human histologic assessment showed that newly formed bone was present at 3 months, and degrees of bone organization increased as time elapsed in vivo. Human histology showed that the material is suitable for bone regeneration in a maxillofacial complex region.

1. Introduction

Form and function replacement of lost hard tissue through guided regeneration with either synthetic materials or tissue engineering (cellular and tissue level regeneration) has been of interest of both healthcare practitioners and patients. The reason for such interest include the avoidance of a second surgical site and procedure (i.e. autologous bone grafting), and the potential secondary infection due to cadaveric (allogenous) and animal (xenogenous) bone processing for grafting purposes [1–3].

Among bioceramics, Ca- and P-based synthetic materials such as hydroxyapatite (HA), β-tricalcium phosphate (β-TCP or $Ca_3(PO_4)_2$), and biphasic blends have been widely utilized in dentistry and orthopedics [4]. These materials have been employed as bone defect filling materials [4,5], implant coatings [6], bone substitutes [7], drug delivery/biologic carriers [8], and resorbable scaffolds [9–13]. These various applications originated due to their degradation followed by bone replacement as time elapses *in vivo* [4,6,14].

During the process of dental or orthopedic function reestablishment, full or partial organ form is desirable in order to improve subsequent load bearing capability [6]. Therefore, characteristics such as Ca- and P-release during wound healing, material packability for appropriate insertion, initial stability, defect filling capability, and dissolution rate comparable to bone healing mineral apposition rate are highly desirable for bone regeneration short- and long-term success [4,6,9,14,15]. To date, no synthetic material has been able to meet all desirable characteristics.

While synthetic pure HA-based bioceramics have been widely used in dental and orthopedic surgical protocols, research has shown high contents of synthetic material remnants in HA-grafted sites after several years *in vivo* [4,6]. The large amount of synthetic material presence in grafted sites may be detrimental to both overall mechanical properties of the regenerated organ and success of subsequent surgical procedures like implant placement. These drawbacks originally related to the use of pure crystalline HA-based bioceramics and led to the rationale for the development of pure phase (pure β-TCP) and blended (HA-β-TCP and HA-α-TCP) bioceramic

* Corresponding author. 345 24th street room 804s, New York, NY 10010, USA. Tel.: +1 646 812 1893.
E-mail address: pc92@nyu.edu (P.G. Coelho).

0928-4931/$ – see front matter © 2009 Elsevier B.V. All rights reserved.
doi:10.1016/j.msec.2009.04.013

materials that present higher degradation kinetics [16–19]. Several studies have demonstrated that pure phase (β-TCP) and blended bioceramic materials (HA-β-TCP and HA-α-TCP) are considered more biologically active when compared to crystalline HA [16,19].

Regarding material solubility, tricalcium phosphates are more soluble under varied media than pure crystalline HA-based materials. The solubility in water of these components are α-TCP>β-TCP>HA [9,20]. From a theoretical standpoint, the release of higher quantities of Ca and P ions into adjacent tissue after surgical placement is desirable for accelerating wound healing [20,9]. This higher dissolution rate of β-TCP compared to pure crystalline HA (3–12 times faster) is related to β-TCP hydrolysis, which occurs in tandem with bone regeneration and depends on the material macro and micromorphology [18]. Therefore, the employment of β-TCP is desirable if higher dissolution and potential bone substitution is intended.

Other factors related to synthetic materials dissolution rate is density, particle and pore size distribution, and surface area [21]. These factors have also been associated with alteration in cell migration and subsequent bone ingrowth into the wound healing site filled by the synthetic material [6]. Fundamentally, an appropriate interplay between physico/chemical variables which influence synthetic materials dissolution may be utilized to achieve tailored *in vivo* materials behavior. Thus, in order to determine a relationship between the host response to grafting materials of different composition and morphology, it is crucial that their physico/chemical properties are well known prior to their clinical trials and subsequent large scale utilization.

The purpose of this study was to evaluate the physico/chemical and the histological characteristic of a β-TCP grafting material grafting material.

2. Materials and methods

An FDA approved beta-tricalcium phosphate (β-TCP) grafting material (SynthoGraft™, Bicon LLC, Boston, USA) was evaluated. The grafting material was provided by the manufacturer and was characterized in the as-received form without any disclosure about its physico/chemical characteristics.

2.1. Physico/chemical analyses

2.1.1. Grafting material morphology

Grafting material morphology was assessed by scanning electron microscopy (SEM, Philips XL30, Eindhoven, The Netherlands), by spreading a minor amount of granules on a double-sided carbon tape. The granules were carbon coated and examined under an accelerating voltage of 15 kV. The particles were also analyzed in a high resolution transmission electron microscope (TEM, Jeol 200 C Japan) operated at 200 KeV. The TEM samples were prepared by ultrasonically dispersing the particles in methanol prior to collection on carbon coated grids.

Grafting material particle size distribution was assessed by means of a scattering-laser technique (Coulter Multisizer and Sample Stand II, Coulter Electronics Limited, Luton, UK). The specific surface area of the particulate material was measured through the multipoint Brunauer-Emmett-Teller (BET) technique by adsorption/disorption of nitrogen (Model No. ASAP 2000, Micromeritics Instrument Corp., Norcross, GA).

Mercury porosimetry (PoreSizer model No. 9320, Micromeritics Instrument Corp., Norcross, GA) was employed to determine pore-size distribution.

2.1.2. Grafting material chemical assessment

Initial semi-quantitative chemical analyses of the grafting material composition was carried out by energy dispersive spectroscopy (EDS, EDAX, Japan), at randomly selected spots, in order to determine the overall approximate calcium and phosphorous ratio.

For surface chemistry assessment, the grafting material samples were inserted into a vacuum transfer chamber and degassed to 10^{-7} Torr. The samples were then transferred under vacuum to a Kratos Axis 165 multitechnique XPS spectrometer. Survey and high resolution spectra were obtained using a 165 mm mean radius concentric hemispherical analyzer operated at constant pass energy of 160 eV for survey and 80 eV for high resolution scans. The particulate material samples were evaluated at various locations.

Fourier-transform infrared spectroscopy (Magna-IR 550 Spectrometer Series II, Nicolet, Madison, WI, USA) equipped with reflectance attachment was used to determine chemical groups and crystallinity and further confirm XRD results. The spectra were collected at room temperature at a nominal resolution of 4.00 and number of sample scans equal to 1000. The FTIR spectra were recorded in the 400–4000 cm^{-1} range using specular reflection.

X-ray powder diffraction patterns (XRD) were collected in a Rigaku diffractometer (Multiflex, Tokyo, Japan), from 5° to 110° (2θ) with step interval $\Delta 2\theta = 0.02°$, divergence slit = 1/2° and receiving slit = 0.3 mm, step time = 8 s, 40 kV, 30ma $CuK_{\alpha 1}$ radiation monocromatized by graphite crystal. Identification of phases was achieved by comparing the diffraction patterns obtained to the database provided by ICDD.

The Rietveld refinements were performed using the GSAS software Collaborative Computacional Project No 14 (CCP14) in powder and Small Molecule Single Crystal Diffraction [22]. The starting model used in refinement was based on the theoretical structure in Inorganic Crystal Structure Data Base (ICSD) [23]. The peak shapes were modeled using the pseudo-Voigt function. The background, cell parameters, preferred orientation, peak asymmetry, atomic positions, site occupancy factors and global vibrational parameters were refined. The calculated and observed patterns were fitted by least squares method until a minimum was reached. The integrated intensities and the peaks heights were related to a scale factor. The fraction of each phase was determined by the equation:

$$W_i = S_i\,(ZMV)_i \,/\, \Sigma\left[\, S_j\left(ZMV_j\right)\right] \tag{1}$$

where:

W_i	weight fraction of the phase p
S	scale factor
Z	number of formulas units per unit cell
M	mass of the formula unit
V	unit cell volume

2.2. Preliminary human histology: surgical procedure, specimen retrieval, and histologic preparation

Following IRB approval from the University of Cartagena, 36 patients with edentulous posterior maxilla without sufficient bone for implant placement were screened. Exclusion factors included local diseases of the musculoskeletal system like TMJ problems, arthritis, and systemic diseases such as problems of the cardiovascular system (hypertension, rheumatic heart desease, cardiac arrhythmia, chronic-heart-failure), respiratory problems (asthma, emphysema), problems of the nervous and endocrine system (depression, neuralgias, diabetes, osteoporosis) and autoimmune diseases or immune deficiency.

A total of 12 of 36 patients met the requirements and were referred to sinus augmentation procedure. An oval osteotomy (aprox.10 mm mesio-distal and 7 mm vertical) of the lateral sinus wall was performed with a 4 mm diameter round bur (Brasseler USA, Savannah, GA) bur at 1300 rpm and external water irrigation. After displacement of the Schneider-membrane the sinus cavity was filled with the beta-TCP which was previously mixed with the patients' blood. The osteotomy was covered with a resorbable collagen membrane (Bicon Resorbable Collagen Membrane, Bicon LLC, Boston, USA) and the full thickness flap was sutured with nylon 3-0.

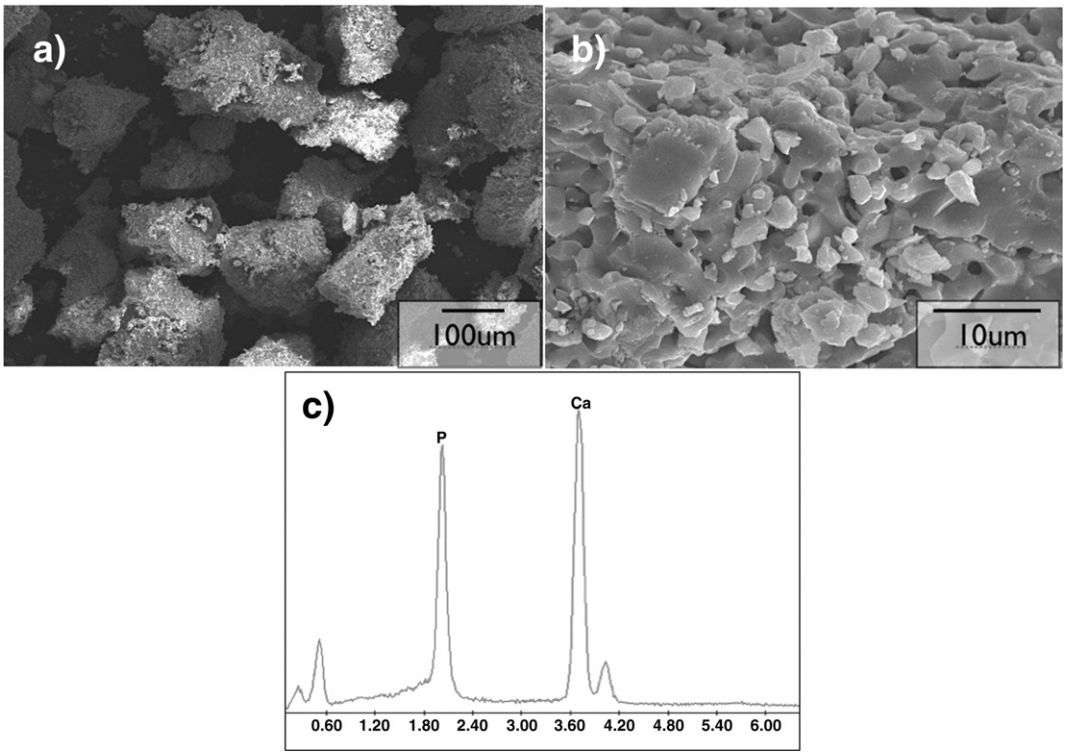

Fig. 1. SEM micrographs: (a) granules morphology; (b) surface characteristic, such as roughness and porosity.(c) EDS spectrum of the powder.

The grafted regions samples were retrieved by means of a trephine bur of 4,75 mm diameter (Bicon LLC, Boston, USA). Samples were collected from each patient at 3, 6, and 9 months after surgery by inserting the trephine bur perpendicular to the occlusal plane to an average depth of 10 mm. The trephined area was prepared with a 6 mm diameter hand reamer and implants (6×5.7 mm) were immediately placed into the donation area. The trephined samples were then placed in 10% buffered formaline solution for 7 days, were dehydrated in a series of graded ethanol (ranging from 70% to 99%), and were paraffin embedded. Thin sections (~5 μm thickness) aiming the central region of the trephined core long axis were produced by means of a microtome. The sections were Hematoxylin and Eosin stained, and their histomorphologic parameters evaluated under an optical microscope (Leica DM 4000, Wetzlar, Germany) in transmitted light mode at various magnifications.

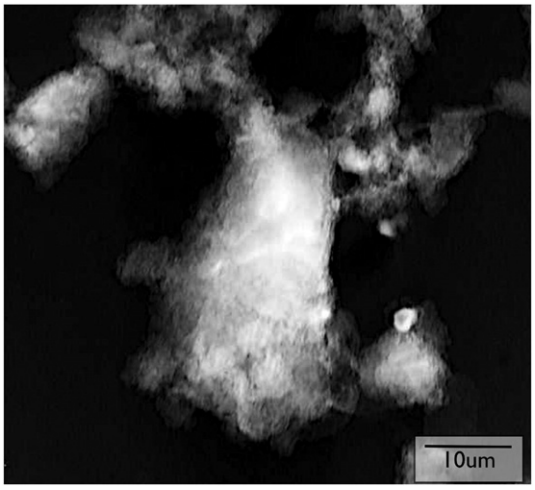

Fig. 2. Representative TEM micrograph of powder particles.

3. Results

Both SEM and TEM micrographs (Figs. 1 and 2, respectively) showed a lathe particle morphology. Intragranular porosity was observed at the ceramic matrix, revealing that the granules were subjected to a sinterization process or a thermal treatment prior to milling to its final particulate material form. A low specific surface area (0.9178 ± 0.03283 m^2/g) was found for the samples through the BET technique. In addition, SEM and TEM micrographs (Figs. 1 and 2) revealed the presence of porosity between particles and rough microstructure of the granule surface. The EDS spectra (Fig. 1) showed that the starting grafting material was generally free of contaminants since only calcium and phosphorous peaks were observed. Representative stoichiometric calculations at different regions showed Ca/P molar ratios ranging from 1.44 to 1.56.

The particle size distribution assessed by means of scattering-laser based techniques showed a polydispersed pattern. The mean diameters of amounts of sample in 10%, 50% and 90% of the total volume are shown in Table 1.

The mercury porosimetry results showed a bimodal pore distribution (Fig. 3). Macro, micrometer, and submicrometer pore distributions were present at the sample (Fig. 3). The picnometry result for the grafting material density was $\rho = 2.87 \pm 0.02$ g/cm^3, which is lower than the theoretical values for β-tricalcium phosphate (3.05 g/cm^3).

The grafting material surface spectra obtained through XPS showed peaks associated to Ca, P, O (531.5 eV), and C (284.8 eV) characteristics orbitals at the particulate material surface. The atomic percentage

Table 1
Range of granules size distribution and mean size assessed by scattering-laser based technique.

Amounts of sample % vol.	Diameter values obtained
D 10%	76.8 μm
D 50%	295.7 μm
D 90%	504.3 μm

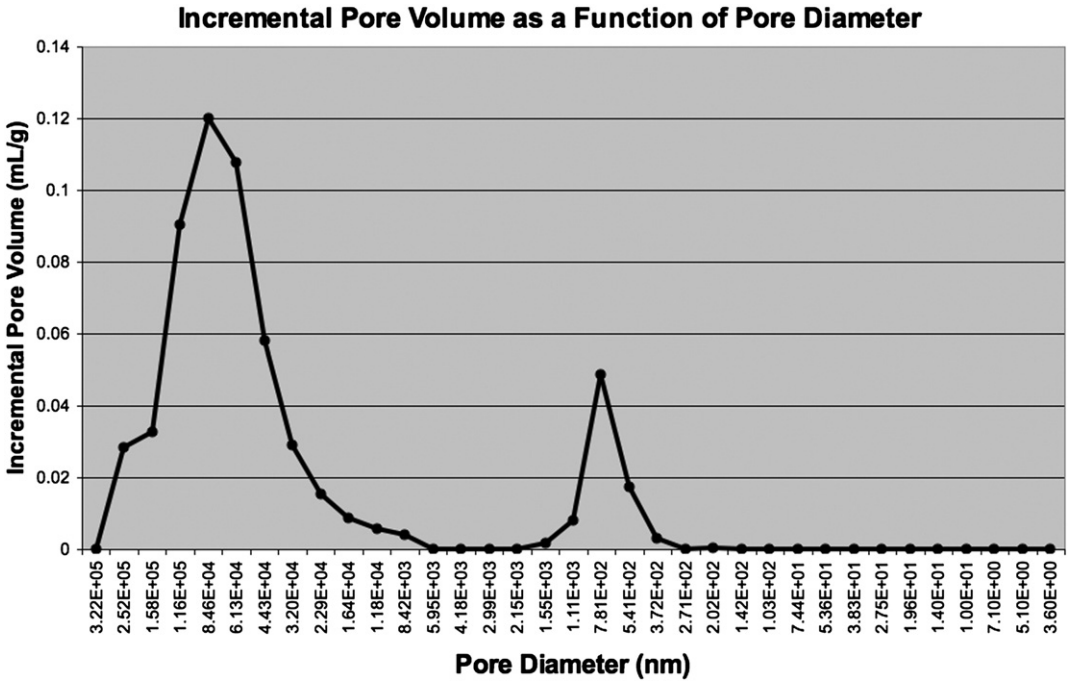

Fig. 3. Pore size distribution curve of the starting material.

(Table 2) of Ca and P 13.6% ± 0.4% and 14.1% ± 0.7%, respectively, leading to a Ca/P ratio of 0.96 at the sample surface.

The FTIR spectra obtained to verify the presence of P–O, P–O–H, H–O–H, α-TCP and β-TCP characteristic bands is presented in Fig. 4. FTIR characteristic bands for β-TCP include a wide band from 900–1200 cm^{-1} [4]. The band at 1650 cm^{-1} was assigned to adsorbed H_2O. The absorption bands at 1092, 1044, 1036, 960, 602, 573, and 475 cm^{-1} were assigned to the vibration in the PO_4^3-group. The presence of a band at 725 cm^{-1} is characteristic for the symmetric mode ν(P–O–P) $P_2O_7^{-4}$. The characteristic peak at 1211 cm^{-1} refers to the non-degenerated flat deformation of hydrogen in groups: $_3$OPO–H–––O–PO_3, common in HPO_4^{-2} ions.

The XRD and final Rietveld plot represented in Fig. 5 displays reasonable agreement between the structural model and the raw data. The results for agreement indexes and phases percentages obtained by the Rietveld method are described in Table 3.

Histologic sections' micrographs taken from the central region of the retrieved cores are presented in Fig. 6. At 3 weeks (Fig. 6a), regions of new bone were evident along with a dense connective tissue. The inclusion of osteocytes in a disordered fashion on the formed bone, characteristic of woven bone, was found along regions where the grafting material remnants occurred. At different regions the grafting material remnants were surrounded by dense connective tissue. At 6 months (Fig. 6b), qualitatively more bone and a substantial increase vascularization along with a decrease in the amount of connective tissue and remaining grafting material was observed. Bone modeling sites were also observed at different regions of the retrieved samples. At 9 months (Fig. 6c), higher degrees of bone organization (lamellar bone regions) were observed along with a qualitative decrease in the grafted region vascularization.

Table 2
Elements amounts found in sample surface characterized by XPS.

Elements	Concentration (at.%)
Ca	13.6 ± 0.4
P	14.1 ± 0.7
O	43.4 ± 0.6
C	28.8 ± 0.3

4. Discussion

The cellular osteogenic response to grafting materials for guided bone regeneration is influenced by the material's chemical composition and surface topography [18]. In order to develop and informed design rationale for the development of future particulate grafting materials, it is crucial that its physicho/chemical properties are well understood prior to laboratory *in vivo* and clinical trials. For this purpose, a series of analytical tools were utilized for the characterization of a commercially available β-TCP grafting material.

The polydispersed, lathe shaped, porous material morphology observed by SEM and TEM analyses has been previously shown to be osteoconductive in large bone defects [6]. It is general consensus that biomaterials' surface roughness plays a significant role on the initial wound healing stages, where molecular and cell attachment detachment dynamics may lead to different healing kinetics [6,26,27]. Specific to implantable materials, past research has reported that rougher surfaces favors osteoblastic attachment [25]. Current developments in the implantology field has devoted significant attention to biomaterials' surface texture and chemistry modification, since it

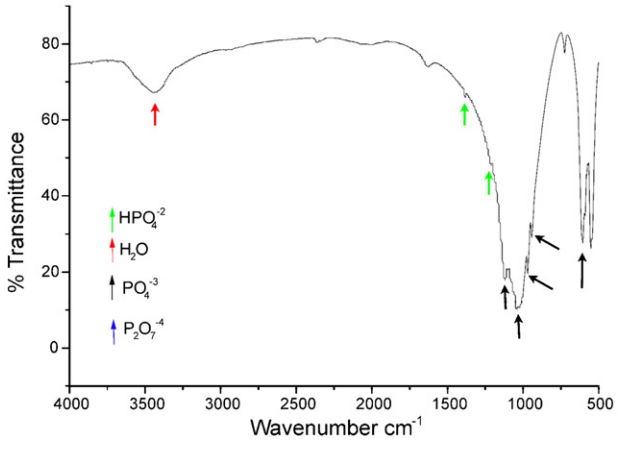

Fig. 4. FTIR spectrum of the as-received powder.

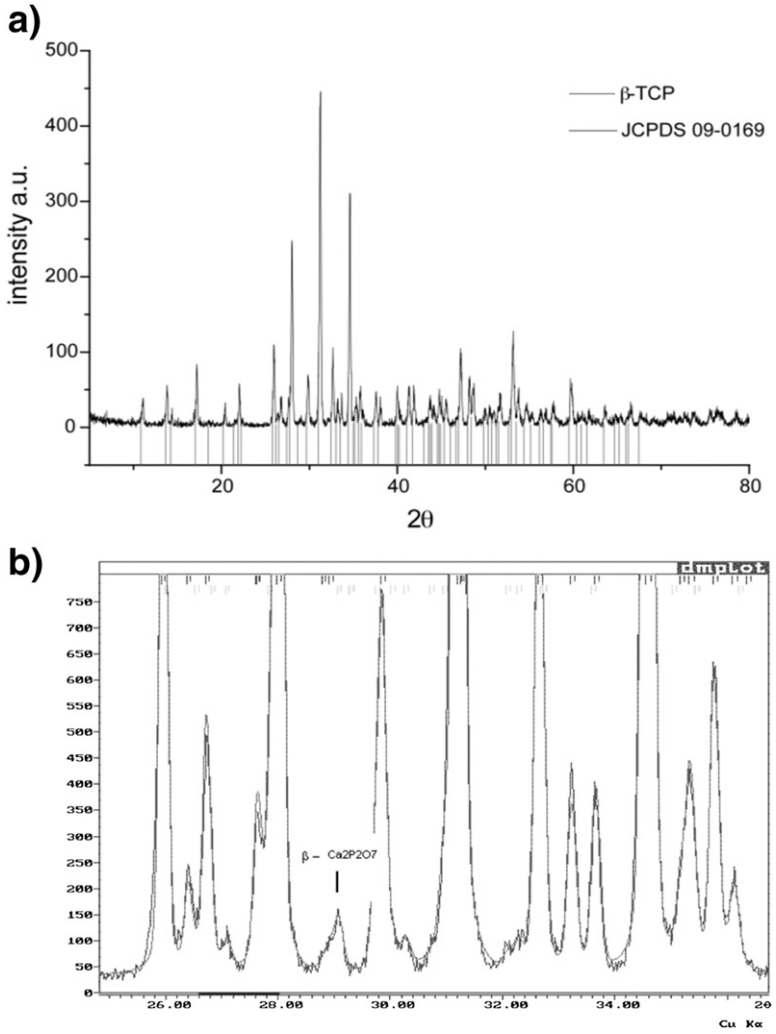

Fig. 5. a. Refinement plot results for the phases β-$Ca_3(PO_4)_2$ and β-$Ca_2P_2O_7$. b. Refinement plot results between 25° and 35° 2θ.

is the first part of the biomaterial which will be exposed to the aggressive wound healing environment [24,25].

The overall chemistry of the material assessed by EDS showed that the calculated molar ratios presented remarkably close stoichiometric Ca/P values when compared to the theoretical β-TCP values in most regions analyzed. In a few instances, the EDS spectrum presented slightly smaller values, which may be attributed to the presence of the other ions in traces amount like, Na, Mg, K, or other phases such as P_2O_7, detected by FTIR and Rietveld method.

The initial *in vivo* ion/biomolecular adsorption that will start the wound healing sequence of biological events that may or not lead to an effective cellular interaction is dependent on the molecular species at or adsorbed at the material surface during manufacturing or just prior to implantation [8]. The XPS results also showed the presence of biocompatible elements in all regions evaluated. The presence of CO_2 at the analysis atmosphere likely contributed for the high concentration of C found at the sample surface. However, the presence of C on the material surface does not imply that such species is present in the bulk material, since no evidence of a specific phase containing C was detected by FTIR, XRD, or Rietveld refinements. The lower amount of Ca at the sample surface can be due to preferential concentration of PO_4^{-3} groups that tend to diffuse to the superficial layers at the nanometric scale. The O and C presence at the material surface are possibly associated to PO_4^{-3} and CO_3^{-2} groups commonly found in calcium phosphates [4,26]. These groups take part of the precipitation process of a phase compatible to the biological environment, and are considered to be the ions responsible for the negative charge maintenance typically found at calcium phosphate materials' surface [18]. The presence of a negative charge associated to these specimens can improve the bioactive property of the material by the electrostatic attraction of selected ions, proteins, and cells, playing a role on the material biocompatible and cytotoxic properties [4].

The absence of 460 and 740 cm^{-1} bands characteristic of α-TCP and an isolated band approximately at 600 cm^{-1} in FTIR showed that the material was high in β-TCP content.

The X-ray patterns collected for calcium phosphates have a great number of superimposed peaks. The Rietveld method resolved the peaks for the quantitative analysis even for low phase's percentages. The most intense Bragg reflection for β-$Ca_2P_2O_7$, according to ICDD data base 9-346 was identified and quantitative analysis for this phase could be performed.

Table 3
Results of the Rietveld refinement for β-$Ca_3(PO_4)_2$ + β-$Ca_2P_2O_7$ sample.

β-TCP			$\tilde{\beta}$- $Ca_2P_2O_7$	
Unit cell parameters	a = b = 10.425 ± 0.000	c = 37.414 ± 0.000	a = b = 6.689 ± 0.000	c = 37.414 ± 0.000
d(g/cm^3)	3.130		3.125	
V(cm^3)	3.521.4 ± 0.2		1080.6 ± 0.2	
Phases percentage	91.04 ± 0.69		8.96 ± 0.86	
R_B	5.40		5.50	
R_{WP}	11.90			
S	1.50			

*R and S indexes [30].

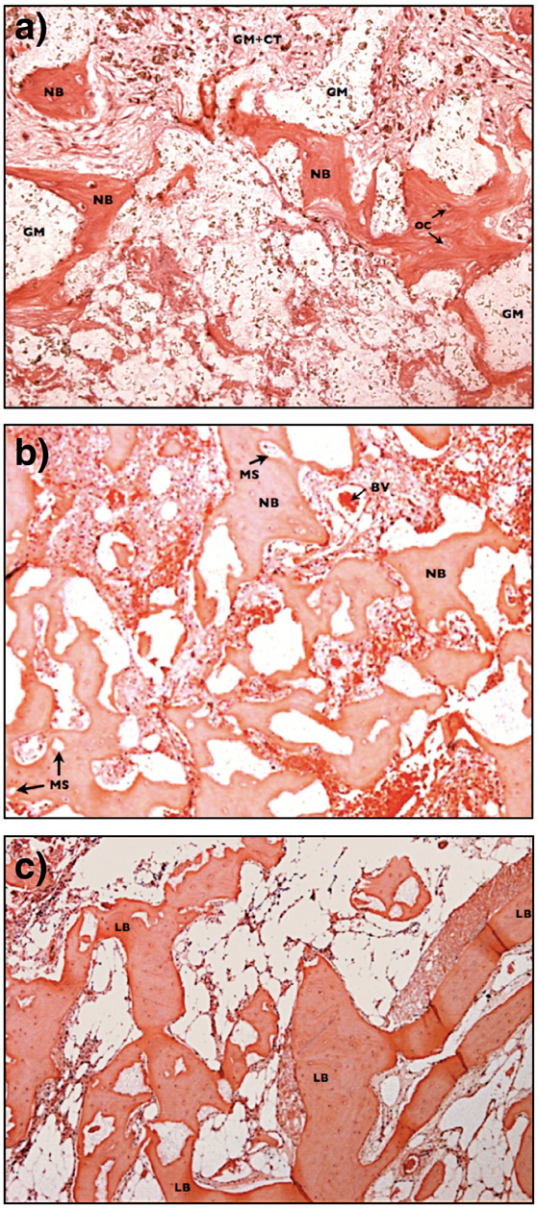

Fig. 6. Histologic sections along the central region of the retrieved human samples. (a) At 3 months, regions of new bone (NB) embedding osteocytes (OC) was evident along with dense connective tissue (CT) regions. The inclusion of osteocytes in the newly formed bone in regions in proximity with remnants of the powder grafting material (GM-dark green particles not totally decalcified during processing) were observed along with regions where grafting material was surrounded by connective tissue (GM + CT). (b) At 6 months, qualitatively more bone was observed along with a substantial increase in the grafted region vascularization (blood vessels-BV) and modeling sites (MS) within newly formed bone (NB). (c) At 9 months, higher degrees of bone organization (lamellar bone regions - LB) were observed along with a qualitative decrease in the grafted region vascularization. (Original mag. 20X, H. and E. Stain).

The spectra obtained in this study were characteristic of β-TCP. However, Rietveld quantitative analysis showed the presence of a secondary phase (β-$Ca_2P_2O_7$). Calcium phosphate crystalline structures generally present complex atomic unit cell distribution and present a challenge for minor phase determination through typical XRD data evaluation set up. Thus, more detailed characterization of minor phase amount or amorphous content is desirable by Rietveld refinement techniques. To date, little documentation of calcium phosphates has been available in the literature. The presence of the small quantity of β-$Ca_2P_2O_7$ determined through Rietveld refinement likely originated from the manufacturing process. Considering a few possible routes for β-TCP synthesis [4]: $2\ CaHPO_4 + 2\ H_2O + Ca_{10}\ (PO_4)_6(OH)_2 \Rightarrow 2\ Ca_3\ (PO_4)_2 + 2\ Ca_2P_2O_7 + 2\ CaO + 6\ H_2O$ or $Ca_{10-x}\ (HPO_4)_x\ (PO_4)_{6-x}\ (OH)_{2-x}$ $(Ca/P = 1{,}50) \Rightarrow 2\ Ca_3\ (PO_4)_2 + Ca_2P_2O_7 + CaO + H_2O$, the presence of a low percentage of $Ca_2P_2O_7$ is expected.

The presence of rapidly dissolving low stoichiometry phases such as β-$Ca_2P_2O_7$ [4] in the particulate is typically not detrimental to the initial host to grafting material. Since the amount of secondary phase determined by Rietveld refinement was considerable (9%), its initial rapid dissolution may enable further opening of the porous network, allowing the release of Ca and P to the wound healing site along with larger diffusivity pathway for nutrients and oxygen which are desirable features for osseoconduction. On the other hand, the release of large quantities of ions at short periods of time may be detrimental or toxic to the dynamically changing cell populating the wound-grafting material [27].

The sequence of events temporally observed in the preliminary human histologic sections are representative of the previously characterized pathway of bone regeneration around different grafting materials [1,7,20]. Initially, an inflammatory response takes place and after several days the grafting material open spaces are filled with connective tissue where osteogenic cells migrate within the wound healing site. Then, new bone is deposited in a disorganized fashion in tandem with the grafting material dissolution, as observed in the 3 months histologic sections. Further bone formation, interconnection, and modeling characteristic of trabecular bone evolution then occurs in tandem with a decrease in the amount of grafting material and an increase in vascularization. Finally, subsequent remodeling resulting in a mature architecture comprising lamellar bone is observed [1,7,20].

While encouraging preliminary histologic findings were obtained, controlled prospective clinical studies are necessary for the proper characterization of the in vivo behavior of the grafting material. Specific to the time frame for implant placement after tissue regeneration, studies concerning implant survival rates are under investigation.

5. Conclusion

The lack of detailed characterization of particulate grafting materials prior to in vivo testing has been limiting the determination of accurate interplays between their properties and biological response. Thus, the informed design rationale of future grafting materials is highly dependent on their physicho/chemical chracterization. The combination of analytical tools showed that the commercially available grafting material evaluated presented crystalline β-TCP particulate material with ~9% β-$Ca_2P_2O_7$ secondary phase concentration. Both bulk and surface chemical analysis were not able to detect contaminants. Finally, human histology showed that the grafting material is suitable for bone regeneration in self-contained defects in the maxillofacial complex, and newly formed bone was detected as early as in 3 months in sinus grafted areas.

Acknowledgements

The authors are grateful for Dr. Ziedonis Skobe from the Forsyth Institute and to Dr. Ana Bressiani from the Materials Science Institute at the Univesity of Sao Paulo's Nuclear and Energetic Research Institute (IPEN).

References

[1] F.C. den Boer, B.W. Wippermann, T.J. Blokhuis, P. Patka, F.C. Bakker, H.J. Haarman, J. Orthop. Res. 21 (2003) 521 no. 3.
[2] S.V. Dorozhkin, M. Epple, Angew. Chem., Int. Ed. Engl. 41 (2002) 3130 no. 17.
[3] A. Krajewski, A. Ravaglioli, Biomaterials 2 (1981) 105 no. 2.
[4] R.Z. LeGeros, Monogr. Oral Sci. 15 (1991) 1.
[5] N. Verdonschot, C.T. van Hal, B.W. Schreurs, P. Buma, R. Huiskes, T.J. Slooff, J. Biomed. Mater. Res. 58 (2001) 599 no. 5.
[6] J.E. Lemons, Bone 19 (1996) 121S no. 1 Suppl.
[7] R.A. Ayers, L.M. Wolford, T.A. Bateman, V.L. Ferguson, S.J. Simske, J. Biomed. Mater. Res. 47 (1999) 54 no. 1.

[8] Y. Liu, K. de Groot, E.B. Hunziker, Ann. Biomed. Eng. 32 (2004) 398 no. 3.
[9] H. Gautier, G. Daculsi, C. Merle, Biomaterials 22 (2001) 2481 no. 18.
[10] C. Zou, W. Weng, X. Deng, K. Cheng, X. Liu, P. Du, G. Shen, G. Han, Biomaterials 26 (2005) 5276 no. 26.
[11] Y. Yin, F. Ye, J. Cui, F. Zhang, X. Li, K. Yao, J. Biomed. Mater. Res. A 67 (2003) 844 no. 3.
[12] N. Rangavittal, A.R. Landa-Canovas, J.M. Gonzalez-Calbet, M. Vallet-Regi, J. Biomed. Mater. Res. 51 (2000) 660 no. 4.
[13] T. Claudio, Methods Enzymol. 207 (1992) 391.
[14] L.L. Hench, Biomaterials 19 (1998) 1419 no. 16.
[15] O. Gauthier, E. Goyenvalle, J.M. Bouler, J. Guicheux, P. Pilet, P. Weiss, G. Daculsi, J. Mater. Sci., Mater. Med. 12 (2001) 385 no. 5.
[16] J.M. Bouler, G. Daculsi, Key Eng. Mater. 192-195 (2001) 119.
[17] G. Daculsi, Biomaterials 19 (1998) 1473 no. 16.
[18] G. Daculsi, R.Z. LeGeros, E. Nery, K. Lynch, B. Kerebel, J. Biomed. Mater. Res. 23 (1989) 883 no. 8.
[19] H. Yuan, K. Kurashina, J.D. de Bruijn, Y. Li, K. de Groot, X. Zhang, Biomaterials 20 (1999) 1799 no. 19.
[20] O. Malard, J.M. Bouler, J. Guicheux, D. Heymann, P. Pilet, C. Coquard, G. Daculsi, J. Biomed. Mater. Res. 46 (1999) 103 no. 1.
[21] K.S. TenHuisen, P.W. Brown, Biomaterials 19 (1998) 2209 no. 23.
[22] G.S.C.C.P.N. (CCP14), "Powder and small molecule single crystal diffraction," 1994.
[23] "Inorganic crystal structure data base (icsd)," U.K., 1995.
[24] A. Wennenberg, T. Albrektsson, Int. J. Prosthodont. 17 (2004) 536 no. 5.
[25] A. Wennenberg, T. Albrektsson, Int. J. Prosthodont. 17 (2004) 544 no. 5.
[26] D. Muster, Demri, M.B. Hage Ali, Enclyc. Handbook of biomaterials and bioengineering, part a, vol. 2, Quintessence Publishing Co., Inc., Chicago, 1995, p. 785.
[27] L.L. Hench, J. Wilson, An introduction to bioceramics, Advanced series in ceramics, vol. 1, World Scientific Publishing Co. Pte. Ltd, Singapore, 1993.